Downloaded from orbit.dtu.dk on: Apr 20, 2024

DTU Library

Multi-level hydrodynamic modelling of a scaled 10MW TLP wind turbine

Pegalajar Jurado, Antonio Manuel; Bredmose, Henrik; Borg, Michael

Published in:
Energy Procedia

Link to article, DOI:
10.1016/j.egypro.2016.09.206

Publication date:
2016

Document Version
Publisher's PDF, also known as Version of record

Link back to DTU Orbit

Citation (APA):
Pegalajar Jurado, A. M., Bredmose, H., & Borg, M. (2016). Multi-level hydrodynamic modelling of a scaled 10MW TLP wind turbine. *Energy Procedia*, *94*, 124-132. https://doi.org/10.1016/j.egypro.2016.09.206

General rights
Copyright and moral rights for the publications made accessible in the public portal are retained by the authors and/or other copyright owners and it is a condition of accessing publications that users recognise and abide by the legal requirements associated with these rights.

- Users may download and print one copy of any publication from the public portal for the purpose of private study or research.
- You may not further distribute the material or use it for any profit-making activity or commercial gain
- You may freely distribute the URL identifying the publication in the public portal

If you believe that this document breaches copyright please contact us providing details, and we will remove access to the work immediately and investigate your claim.

Available online at www.sciencedirect.com

ScienceDirect

Energy Procedia 94 (2016) 124 – 132

Energy Procedia

13th Deep Sea Offshore Wind R&D Conference, EERA DeepWind'2016, 20-22 January 2016, Trondheim, Norway

Multi-level hydrodynamic modelling of a scaled 10MW TLP wind turbine

Antonio Pegalajar-Jurado[a,*], Henrik Bredmose[a], Michael Borg[a]

[a]*DTU Wind Energy, Nils Koppels Allé, building 403, 2800 Kgs. Lyngby, Denmark*

Abstract

In the present paper the accuracy of three numerical models for a scaled 10MW TLP wind turbine is assessed by comparison with test data. The three models present different levels of complexity, and therefore different degrees of accuracy can be expected. A set of load cases including irregular and focused waves is run in the three models, where only wave loads are considered. The simulation results are compared against the test data, and the numerical models are assessed based on their ability to reproduce the test results. Finally, the possibility of enhancing the simple model by using the advanced models is discussed.

© 2016 The Authors. Published by Elsevier Ltd. This is an open access article under the CC BY-NC-ND license (http://creativecommons.org/licenses/by-nc-nd/4.0/).
Peer-review under responsibility of SINTEF Energi AS

Keywords:
hydrodynamic modelling, floating wind turbine, TLP, tension leg platform, wave loads, dynamic response

1. Introduction

The design of floating substructures for offshore wind turbines relies on accurate and trustworthy aero-hydro-servo-elastic numerical models, which in turn must be validated against tests. The initial stages of conceptual design require fast models to quickly evaluate the performance in a broad range of environmental conditions, and to allow for optimization. In later stages more accurate — and thus also more computationally extensive — models are needed. Ideally, models at different levels of accuracy can be combined to form a flexible framework for robust design. Such a framework is being developed as part of LIFES50+ [1], a Horizon 2020-funded project that focuses on the design of the next generation of floaters for 10MW offshore wind turbines.

In this paper three numerical models with different levels of complexity are applied to a scaled version of the DTU 10MW wind turbine [2] mounted on a Tension Leg Platform (TLP), built as part of the INNWIND.EU project [3] and described by Hansen and Laugesen [4] and Bredmose et al. [5], see Fig. 1. A state-of-the-art model with first-order wave kinematics and Morison forcing has recently been compared to experimental data by Pegalajar-Jurado

* Corresponding author
E-mail address: ampj@dtu.dk

1876-6102 © 2016 The Authors. Published by Elsevier Ltd. This is an open access article under the CC BY-NC-ND license (http://creativecommons.org/licenses/by-nc-nd/4.0/).
Peer-review under responsibility of SINTEF Energi AS
doi:10.1016/j.egypro.2016.09.206

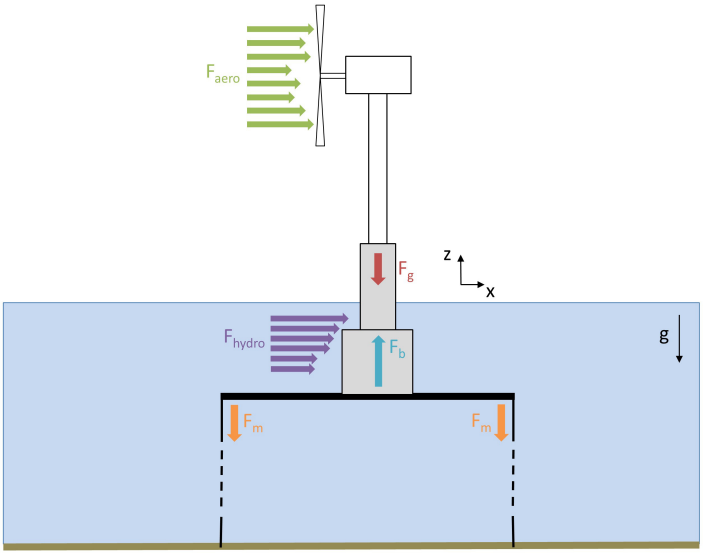

Fig. 1. Simple sketch of a TLP wind turbine in its equilibrium position and the main loads acting on it: aerodynamic (green), gravitational (red), buoyancy (blue), hydrodynamic (purple) and mooring loads (orange).

[6]. In the present work we go one step further, and study the performance of two additional models: a simple, fast frequency-domain model; and an extended version of the state-of-the-art model that includes second-order wave kinematics. The accuracy of the three models is assessed by running a set of load cases where only wave loads are considered. The simulation results are compared and benchmarked against test data. Next, the possibility of utilizing results of the advanced models to enhance the simple models is discussed. The aim of this interconnection between multi-level numerical models and test data is to add reliability to the design tools, ultimately contributing to the reduction of the Levelised Cost Of Energy (LCOE) for floating offshore wind power.

2. Description of models and environmental conditions

The three numerical models are developed around the experimental setup described in [4], and all the comparisons with tests are done in model scale. For each test, the motion of the TLP in its six degrees of freedom is available, as well as the nacelle acceleration and the surface elevation measured by wave gauges at different locations in the wave basin. The TLP wind turbine and environmental conditions are Froude-scaled. Therefore length, time and mass for the full-size model (L, T and M) are related to length, time and mass of the scaled model (l, t and m) as follows:

$$L = l\lambda; \qquad T = t\sqrt{\lambda}; \qquad M = m\lambda^3\rho_{sw}/\rho_{fw} \tag{1}$$

where $\lambda = 60$ is the geometric scaling factor, and ρ_{sw} and ρ_{fw} are the densities of seawater and fresh water, respectively. The scaling of the remaining dynamic quantities can be derived from the scaling of the ones above. The three numerical models, tailored to the scaled TLP wind turbine used for the tests, can be re-casted into the formulation:

$$(\mathbf{M} + \mathbf{A})\ddot{\mathbf{x}}(t) + \mathbf{B}\dot{\mathbf{x}}(t) + \mathbf{C}\mathbf{x}(t) = \mathbf{F}(t, \mathbf{x}) \tag{2}$$

where $\mathbf{M}$, $\mathbf{A}$, $\mathbf{B}$ and $\mathbf{C}$ are the mass, added mass, damping and restoring matrices, respectively. $\mathbf{A}$ and $\mathbf{B}$ are generally frequency-dependent but they are often taken as constants when Morison forcing is used. The position vector of the TLP wind turbine is denoted as $\mathbf{x}(t)$, and $\mathbf{F}(t, \mathbf{x})$ refers to the loads acting on the structure (see Fig. 1). The TLP is stiff in pitch, therefore the natural frequencies of interest for the scaled TLP wind turbine are surge (0.19 Hz) and coupled

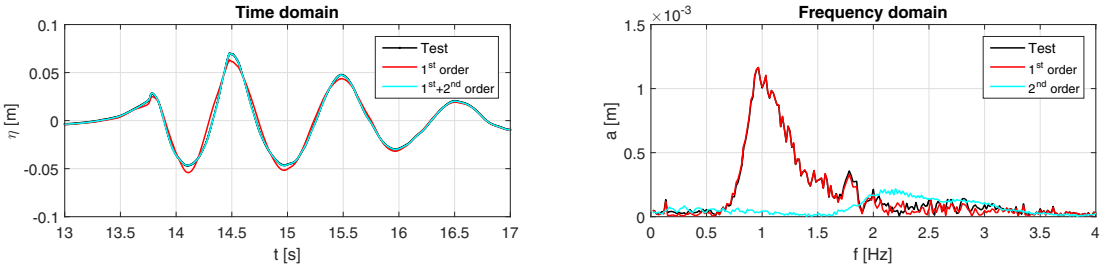

Fig. 2. Surface elevation (left) and wave amplitudes (right) from test and computed with first- and second-order methods.

pitch/tower mode (1.9 Hz). Although based on the same general equation of motion, the different models present different degrees of complexity:

- The simple, frequency-domain model is implemented in *Matlab* with two degrees of freedom: floater surge and nacelle fore-aft displacement. The wave kinematics are computed with Airy theory [7] from the measured surface elevation, and the forcing with the Morison equation [8]. Being a frequency-domain model, the drag term in the Morison equation is computed solely with the wave velocity $u(z)$, in contrast to the widely-used approach of using the relative velocity between water and structure, $(u(z) - \dot{x}(z))$. The difference in drag force arising from this simplification is compensated in the model by rectifying the damping matrix **B** in the equation of motion accordingly. The mooring system is modelled as a single linear spring.

- The state-of-the-art, time-domain model is *Flex5* [9] and includes 28 degrees of freedom, six of which belong to the floater motion: surge, sway, heave, roll, pitch and yaw. The wave forcing is computed with the Morison equation. The mooring system is modelled by considering the tendons as springs and computing their elongation from the fairlead positions. Two versions of this model are employed: one with first-order wave kinematics; and another with second-order wave kinematics computed with the method described by Dean and Sharma [10]. For each simulation the time series of surface elevation measured in the corresponding test is separated into first- and second-order and used to generate the corresponding first- and second-order wave kinematics (see Fig. 2).

For the three models the wave kinematics were computed up to the still water level. The Morison hydrodynamic force was obtained by integration up to $z = 0$ and the addition of a point force F_0 that represents the contribution of the hydrodynamic force on the wet portion between still water level and instantaneous free surface elevation η:

$$F_0 = \eta \left[\rho C_m A u_t + 0.5\rho C_D D|u|u\right]_{z=0} \tag{3}$$

where ρ is the water density, C_m and C_D are the added mass and drag coefficients, A and D are the floater cross-sectional area and diameter at sea water level and u_t and u are the wave acceleration and velocity at $z = 0$. We note that hereby the force associated with first-order wave kinematics is not strictly linear. A similar argument, however, applies to the Morison drag term which also represents a contribution beyond first-order magnitude.

A summary of the key features for the three models is presented in Table 1, where DoF stands for Degrees of Freedom and the sixth column indicates whether the drag term in the Morison equation is calculated with the wave velocity $u(z)$ or with the relative velocity between water and structure $(u(z) - \dot{x}(z))$. Since the focus of the present study is on the hydrodynamics, a set of load cases without wind is chosen. Both irregular and focused waves are used, with the characteristics presented in Table 2. In the table, H_s and T_p are respectively significant wave height and peak period for irregular waves, while H_{max} is the wave height for focused waves (chosen to be nominally $1.86H_s$ for the corresponding 3-hour sea state). The load cases I1 and F1 (irregular; focused) correspond to sea states associated with the rated wind speed of the turbine, while load cases I2 and F2 correspond to a storm condition with idling turbine.

Table 1. Characteristics of the three numerical models employed for the simulations.

Model	DoF (total)	DoF (floater)	Wave kinematics	Wave forcing	Velocity in drag	Mooring system
Matlab	2	1	1st order	Morison	$u(z)$	Single linear spring
Flex5-1st	28	6	1st order	Morison	$(u(z) - \dot{x}(z))$	4 nonlinear springs
Flex5-2nd	28	6	2nd order	Morison	$(u(z) - \dot{x}(z))$	4 nonlinear springs

Table 2. Scaled environmental conditions (in parentheses the corresponding full scale values).

Load case	Type of wave	Duration [s]	H_s [m]	T_p [s]	H_{max} [m]
I1	Irregular	600 (4647)	0.078 (4.68)	0.95 (7.36)	-
I2	Irregular	600 (4647)	0.179 (10.74)	1.60 (12.39)	-
F1	Focused	60 (464.8)	-	-	0.117 (7.02)
F2	Focused	60 (464.8)	-	-	0.314 (18.84)

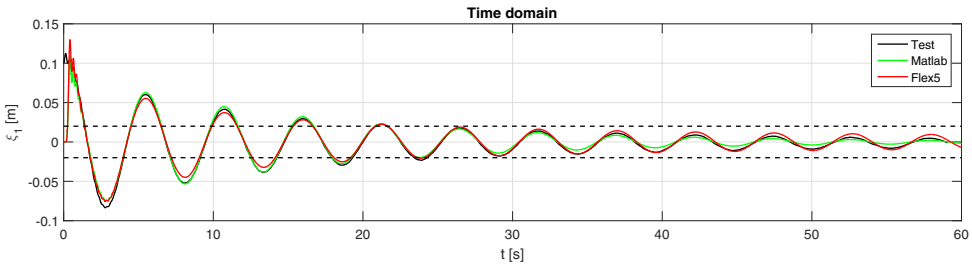

Fig. 3. Decay in surge. The dashed lines bound the region of typical surge range.

3. Calibration of models

The hydrodynamic coefficients in the *Matlab* and *Flex5* models were calibrated by running a surge decay simulation and comparing the response to the surge decay test (see Fig. 3). Since the damping ratio in the drag-damped models is not completely independent of amplitude, a particular effort was made to match the surge decay response to the test in the region of typical surge range, bounded by dashed lines in Fig. 3. The surge natural frequency of the models was matched to that of the test by adjusting the added mass coefficient to $C_m = 0.76$ for the *Matlab* model and $C_m = 0.765$ for *Flex5*. The damping was first tuned in *Flex5* by adjusting the drag coefficient to $C_D = 1.7$. This value of drag coefficient was imported to the *Matlab* model, and the first element of its damping matrix (B_{11}, corresponding to surge motion) was chosen to best reproduce the surge decay response as in Fig. 3.

Further tuning of the *Matlab* model was carried out by comparing the nacelle acceleration with the one predicted by the *Flex5* model for irregular sea state I1 (Fig. 4, bottom). The *Matlab* model does not include platform pitch motion, therefore the tower flexibility EI was adjusted to 2.12 kNm^2 so the nacelle acceleration in the *Matlab* model contains energy at the coupled pitch/tower natural frequency (1.9 Hz). This way the absence of pitch in the simple model is compensated. The second element of the damping matrix (B_{22}, which corresponds to the nacelle displacement) was also tuned to match the nacelle acceleration with the one predicted by the *Flex5* models for irregular sea state I1.

4. Discussion of results

The comparison between models and with test data is carried out in terms of floater surge ξ_1 and nacelle acceleration in the fore-aft direction a_{nac}. The results are presented in terms of time series and Power Spectral Density (PSD) of three signals: surface elevation η; floater surge ξ_1; and nacelle acceleration a_{nac}. For clarity, only a significant time window is shown in the time plots. To avoid the effect of transients in the cases with irregular waves, the PSD plots were obtained by applying the Fast Fourier Transform (FFT) to only the central third of the corresponding time signal.

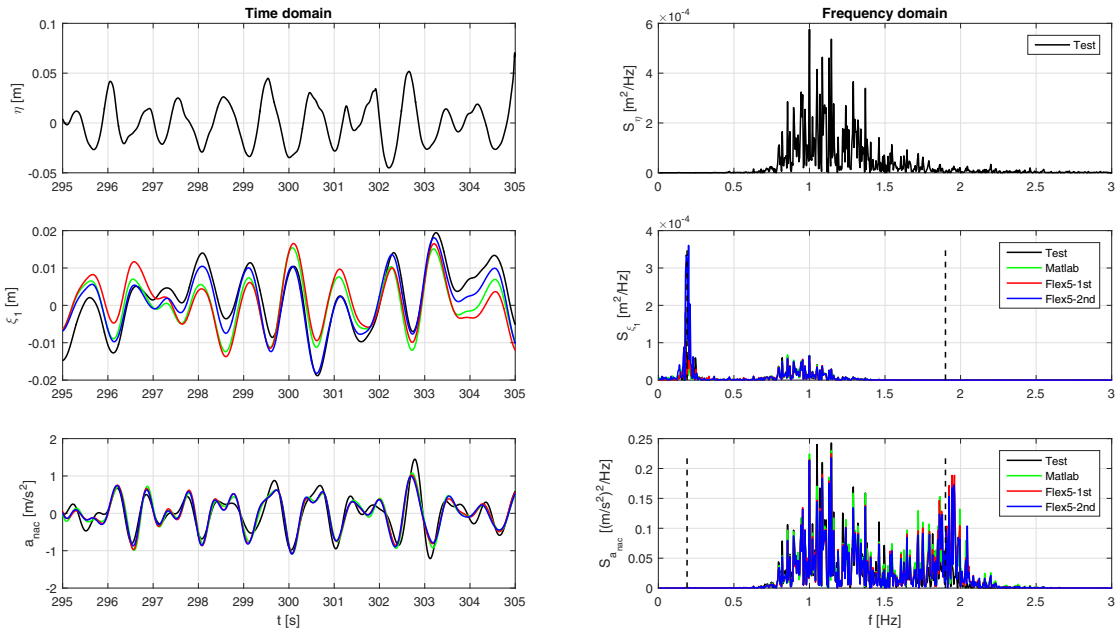

Fig. 4. Time series and PSD, irregular sea state I1. The dashed lines represent the natural frequencies in surge (0.19 Hz) and coupled pitch/tower (1.9 Hz).

For irregular waves a further analysis based on exceedance probability is made, in order to compare the peaks in each of the response signals. First, for each individual wave, the peak of each response signal is stored. Then the peaks are sorted from minimum to maximum and assigned an exceedance probability P_{exc} based on their position in the list. The exceedance probability represents the probability of a particular extreme value being exceeded, therefore the most extreme peaks correspond to the lowest probabilities.

4.1. Results for irregular waves

The response to the irregular sea state I1 is shown in Figures 4 and 5. The surge motion (Fig. 4, middle) presents energy both around the peak wave frequency (1.05 Hz) and at the surge natural frequency (0.19 Hz). The *Matlab* model predicts a smaller surge motion, and both the first- and second-order *Flex5* models are very close to the test for a wide range of probabilities. However, the second-order *Flex5* model shows much more energy at the surge natural frequency, likely due to subharmonic forcing from the second-order wave kinematics. This effect also explains some of the largest extreme values in the exceedance probability plot (Fig. 5, left). Regarding nacelle acceleration (Fig. 4, bottom), the test and all models show energy mainly around the wave peak frequency (1.05 Hz) and at the coupled pitch/tower natural frequency (1.9 Hz). In the exceedance probability plot (Fig. 5, right) all models are very close to each other and to the test, but the second-order *Flex5* model slightly underpredicts the acceleration for probabilities between 0.2 and 0.02. However, since the only difference between the two *Flex5* models is the wave kinematics, a small difference between these models is expected in nacelle acceleration, due to the large inertia of the TLP wind turbine. In addition, due to deep water conditions, superharmonics are diminishing in the limit of infinite depth, and therefore no particular superharmonic forcing is observed around the coupled pitch/tower natural frequency for the second-order *Flex5* model. The damping in the *Matlab* model was tuned so the nacelle acceleration matched the one predicted by *Flex5* in this case, hence a good level of agreement is expected.

Figures 6 and 7 show the system response to the irregular sea state I2, corresponding to a storm condition. In this case the surge response (Fig. 6, middle) also shows energy around the wave peak frequency (0.63 Hz) and at the surge natural frequency (0.19 Hz). Although the peak around surge natural frequency for the second-order *Flex5* model is

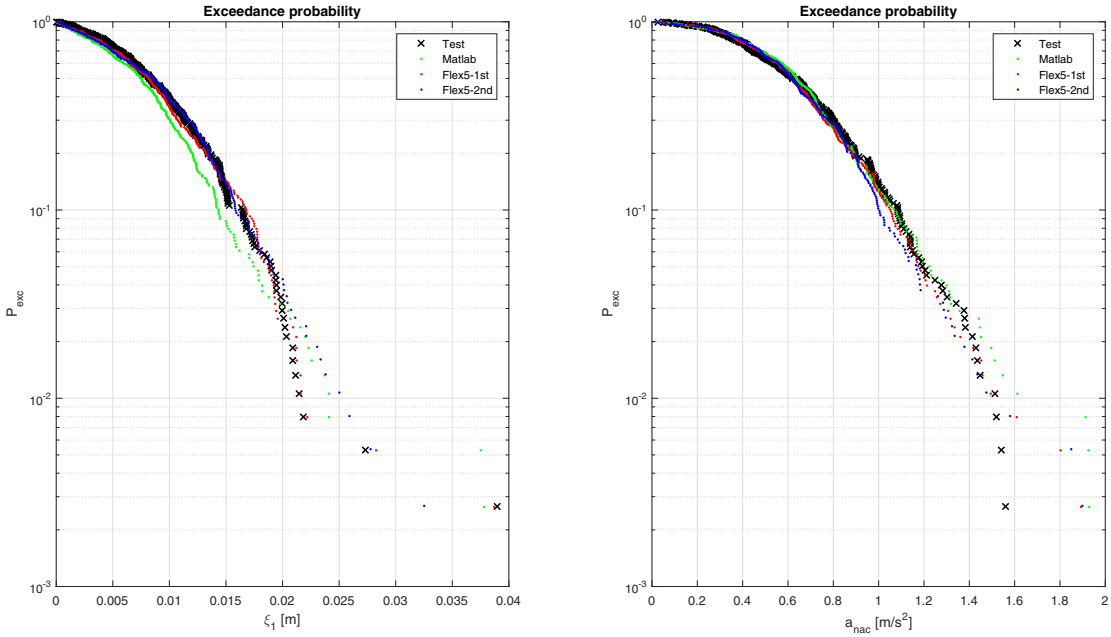

Fig. 5. Exceedance probability, irregular sea state I1.

larger than for the irregular sea state I1, it is relatively smaller when compared to the energy at the wave frequency range. In the exceedance probability plot (Fig. 7, left) all models are close to the test in this case, but this time the surge is overpredicted by all models (and especially by the *Matlab* model) for exceedance probabilities below 0.1. For nacelle acceleration (Fig. 6, bottom) the frequency response is dominated by the wave frequencies for all models, and some energy is also present at the coupled pitch/tower natural frequency (1.9 Hz). In the exceedance probability plot (Fig. 7, right) all models are again close to each other, but this time further away from the test. The underprediction of nacelle acceleration is likely due to the flexibility of the TLP spokes in the experimental setup, which was not included in the numerical models.

4.2. Results for focused waves

Given that focused waves induce a time-localised response, the FFT analysis to obtain the PSD plots is performed on the portion of the time series shown in the time plots. The response to the focused wave F1 can be seen in Fig. 8. The surge response of the structure initially is at the primary wave frequency (1.05 Hz), followed by free oscillations at the surge natural frequency (0.19 Hz) after the free surface movement diminishes. However, the energy at the surge frequency for the first-order *Flex5* model seems significantly higher than for the other models, which present almost the same amount of energy as the test at the surge natural frequency (0.19 Hz). In the time series all three models agree with the test until the second large peak (around 15 s). From this moment, the responses of the *Matlab* and the first-order *Flex5* models deviate from the test. The second-order version of the *Flex5* model is the one to best reproduce the test signal throughout the whole time series, although a small phase difference is observed after 20 s. In nacelle acceleration the energy is mainly centered around the wave frequencies and the coupled pitch/tower natural frequency (1.9 Hz). In the time series and PSD plot it is observed that all the models agree better with each other than with the test, showing a larger amount of energy at high frequencies. The *Matlab* model presents the highest peak around 1.8 Hz, which could be attributed to the method in which the tower flexibility is increased to compensate the absence of floater pitch in this model.

Figure 9 presents the response to the focused wave F2. As in the previous case, the surge natural frequency is visible in the surge motion. The first-order *Flex5* model agrees with the test in the amount of energy at the surge

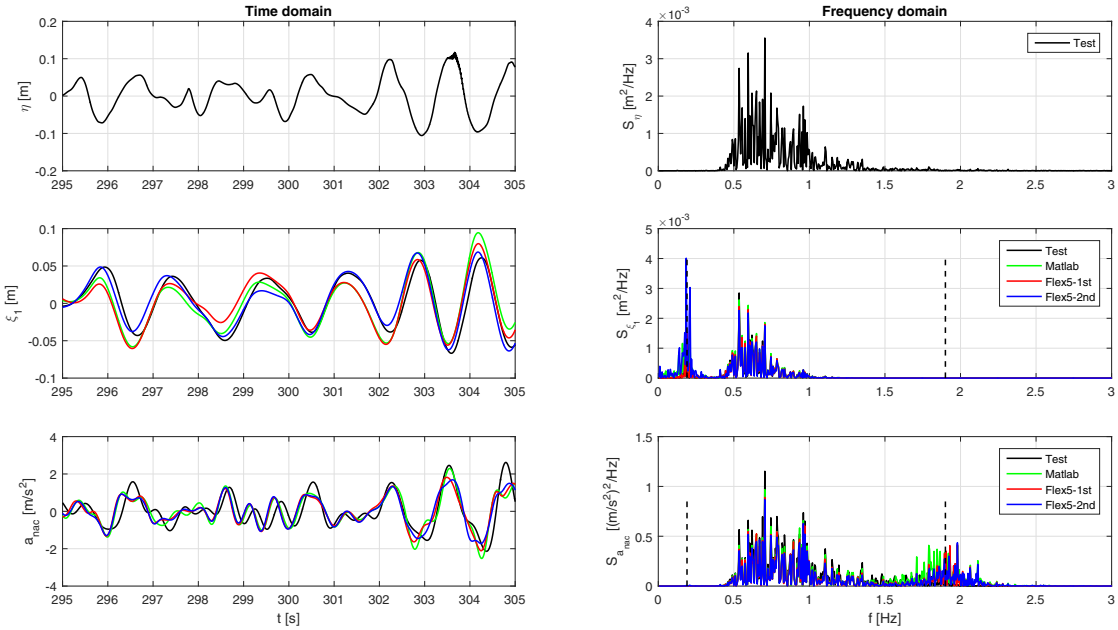

Fig. 6. Time series and PSD, irregular sea state I2. The dashed lines represent the natural frequencies in surge (0.19 Hz) and coupled pitch/tower (1.9 Hz).

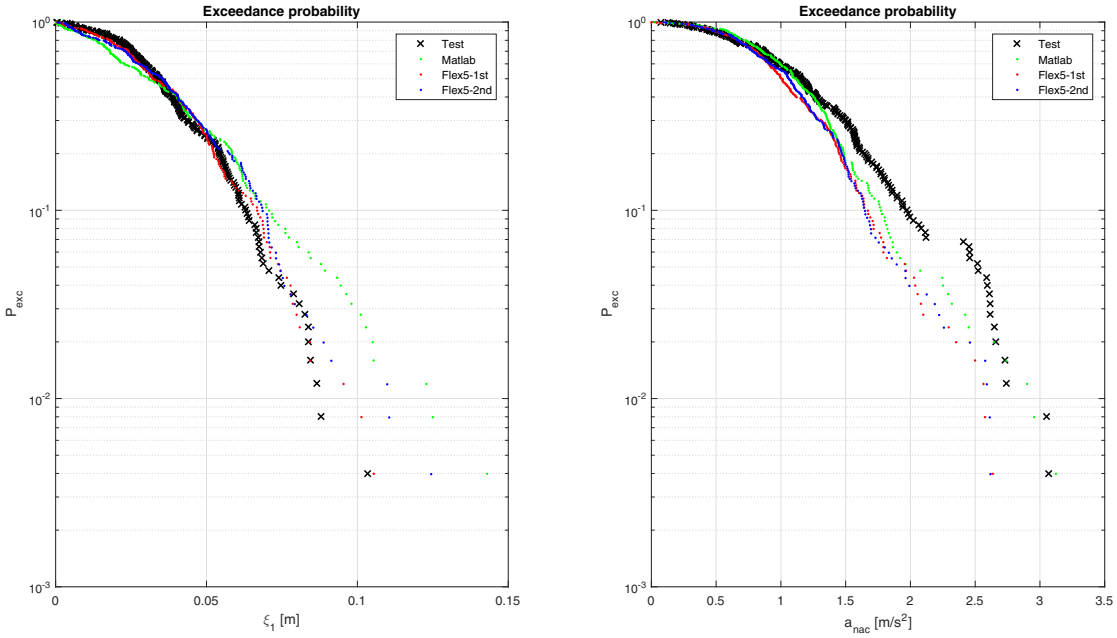

Fig. 7. Exceedance probability, irregular sea state I2.

frequency, whilst the second-order version underpredicts it and the *Matlab* model overpredicts it. The energy around the wave peak frequency (0.63 Hz) is more dominant in this case. In the time series of surge, a decent agreement is observed between both *Flex5* models and the test, while the *Matlab* model overpredicts the two main peaks. As it was

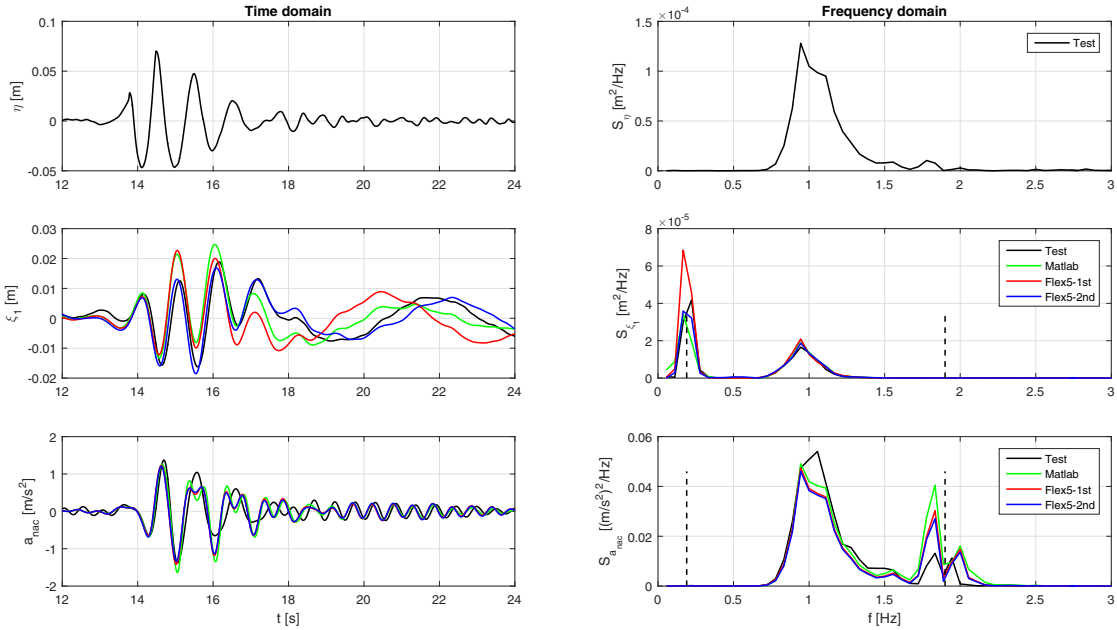

Fig. 8. Time series and PSD, focused wave F1. The dashed lines represent the natural frequencies in surge (0.19 Hz) and coupled pitch/tower (1.9 Hz).

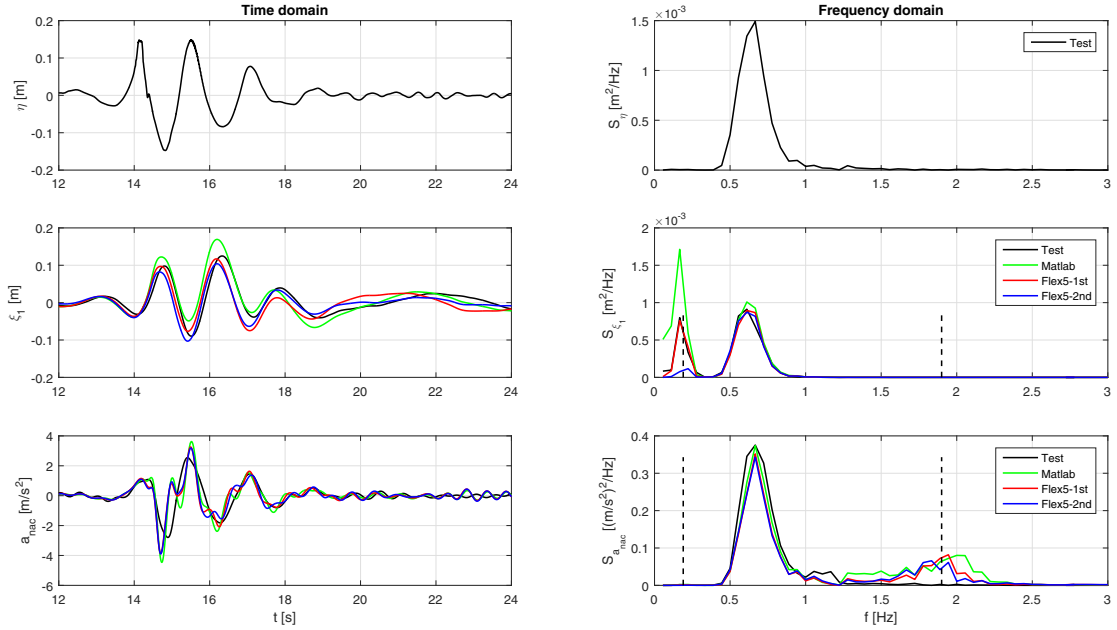

Fig. 9. Time series and PSD, focused wave F2. The dashed lines represent the natural frequencies in surge (0.19 Hz) and coupled pitch/tower (1.9 Hz).

observed for focused wave F1, in nacelle acceleration all models present a response with a high-frequency component at the coupled pitch/tower frequency that is not observed in the test.

5. Conclusions

Given the trade-off between accuracy and computational cost, the simple - and fast - models are expected to yield more coarse results than more advanced - and more computationally expensive - models. In the present study this expectation was partially confirmed. In surge, the simple model performed worse than its more complex equivalents for all cases. However, for nacelle acceleration it presented a similar or even better performance than the *Flex5* models, presumably because the simple model was enhanced with this goal.

For the tests presented, the extension of the *Flex5* model to include second-order wave kinematics was not found to have a great impact on nacelle acceleration, as the effect is negated by the large inertia of the TLP wind turbine. Also, the condition of deep water tends to diminish the superharmonics in the second-order wave kinematics, which could potentially excite the pitch motion and increase the motion of the nacelle. A greater impact of the wave kinematics is observed on the surge motion, leading to a better prediction of surge motion in most cases, as expected given the more accurate description of the wave kinematics when including the sub-harmonic and super-harmonic second-order contributions. One thing to note here is the difference between the test conditions in the laboratory with first-order paddle motion and spatial development of second-order wave energy and the steady amplitude assumption of closed-form second-order wave theory.

Finally, the more advanced numerical models have been employed to enhance the simple one. Given the absence of pitch motion in the *Matlab* model, it originally underpredicted nacelle acceleration. The stiffness of the tower was reduced to recreate the same frequency in the nacelle motion as in the *Flex5* models, and the damping was adjusted towards obtaining the same nacelle acceleration as with *Flex5*. These modifications resulted in a much better performance of the simple model, which is now comparable to the more advanced models in the cases presented in this study. This research thus illustrates how models of different fidelity can be combined to allow fast load assessment with simple models in early design stages, and later more accurate design through the more advanced models.

Acknowledgements

This work is part of the project LIFES50+ [1]. The research leading to these results has received funding from the European Union's Horizon 2020 research and innovation programme under grant agreement No. 640741. The experimental results were obtained as part of the INNWIND.EU project [3].

References

[1] LIFES50+ project. *URL: http://www.lifes50plus.eu.* [Accesed 07-01-2016].
[2] Bak C, Zahle F, Bitsche R, Kim T, Yde A, Henriksen LC, Andersen PB, Natarajan A, Hansen MH. Description of the DTU 10 MW Reference Wind Turbine. DTU Wind Energy Report-I-0092, Roskilde, Denmark, 2013.
[3] INNWIND.EU project. *URL: http://www.innwind.eu.* [Accesed 04-01-2016].
[4] Hansen AM, Laugesen R. Experimental study of the dynamic response of the DTU 10MW wind turbine on a tension leg platform. MSc thesis, DTU Wind Energy. Kgs. Lyngby, Denmark, 2015.
[5] Bredmose H, Mikkelsen RF, Hansen AM, Laugesen R, Heilskov N, Jensen B, Kirkegaard J. Experimental study of the DTU 10 MW wind turbine on a TLP floater in waves and wind. Presented at EWEA Offshore 2015 Conference. Copenhagen, Denmark, 2015.
[6] Pegalajar-Jurado A. Numerical reproduction of laboratory experiments for a TLP wind turbine. MSc thesis, DTU Wind Energy. Kgs. Lyngby, Denmark, 2015.
[7] Airy GB. Tides and waves. In: Smedley E, Rose HJ, Rose HJ, editors. *Mixed Sciences*, vol. 3. London: Encyclopaedia Metropolitana;1845. p. 241*-396*.
[8] Morison JR, O'Brien MP, Johnson JW, Schaaf SA. The force exerted by surface waves on piles. *Petroleum Transactions (AIME)* 1950;189:149-154.
[9] Øye S. FLEX4 simulation of wind turbine dynamics. In: *Proceedings of the 28th IEA meeting of experts concerning state of the art of aero-elastic codes for wind turbine calculations* (Available through IEA) 1996; 129-135.
[10] Sharma JN, Dean RG. Second-order directional seas and associated wave forces. *Society of Petroleum Engineers Journal*, 1981;21(01):129-140.